Dual Ascent Algorithm-Based Improved Droop Control for Efficient Operation of AC Microgrid

Yajie Jiang[1] and Yun Yang[2]*

[1]*Department of Electrical and Electronic Engineering, The University of Hong Kong, Pokfulam, Hong Kong SAR, China,*
[2]*Department of Electrical Engineering, The Hong Kong Polytechnic University, Kowloon, Hong Kong SAR, China*

In this work, the loss (including wire loss and converter loss) of island three-phase AC microgrid is modeled as a quadratic function of the current distribution coefficient, that is, a concave function with equality and inequality constraints. On the basis of the concave optimization principle, the optimal current distribution coefficient of the distributed energy unit (DEU) is calculated online by the double ascent optimization method (DAOM) to minimize the distribution loss. It is proven that the concave function with multi-variables can be optimized by the DAOM. Using the average reactive power distribution scheme, the optimal active power distribution coefficient with the minimum distribution loss of the AC microgrid can be obtained in real time. In addition, given the high R/X ratio in the short-distance AC microgrid, the active power–frequency (P-ω) droop control and reactive power–voltage amplitude (Q-E) droop control are not suitable for power distribution among DEUs. Thus, an advanced strategy comprising active power–voltage amplitude (P-E) droop control and reactive power-frequency (Q-ω) droop control is proposed to dispatch the output active powers and reactive powers of DEUs. Simulation examples are provided to verify the convexity of the proposed model and the effectiveness of the control strategy.

Keywords: AC microgrid, concave optimization, distributed energy unit (DEU), distribution loss, double ascent optimization method (DAOM)

INTRODUCTION

To reverse the trend of the greenhouse effect and reduce carbon emission, reducing loss in modern grid systems is an important research topic (Qian et al., 2020; Jiang et al., 2021a; Li and Roche, 2021). Theoretically, the power loss in the grid can be expressed by the function of the wire resistance matrix and node voltages of distributed energy units (DEUs). Thereby, some studies are carried out on the basis of the wire loss model, such as bus voltage searching (Jiang et al., 2021b) and power flow distribution (Yang et al., 2019). This traditional loss model is easy to change due to the influence of temperature and humidity. Furthermore, only the wire loss can be reduced, whereas the loss of the power converter is not considered. In fact, in an AC microgrid, converter loss may occupy over 50% of the total loss in the distribution network system (Beerten et al., 2012). Therefore, taking this part of loss into account in the control scheme is very important for minimizing the power loss in the distribution network.

Distribution Loss Modelling

As introduced in many research studies and technical manuals, the loss of power in a power electronics converter can be described as a function of the output power. It has been studied in some research works. In the study by Yuan et al. (2021a), the converter loss is further approximated as a

quadratic function by the output powers of DEUs. Then, the output active powers and reactive powers of the individual converter are dispatched by the concave allocation algorithm. In the study by Wang et al. (2010) and Teng et al. (2016), one converter-discarding strategy is used to adjust the number of operating converters. In this way, the overall efficiency of parallel-connected inverters is improved according to the demanding power. However, in these works, the potential for reducing converter loss has not been fully developed (Yuan et al., 2021b). Therefore, considering this in the control scheme is very important to minimize the power loss in the distribution network. For the AC microgrid with parallel DEUs, the output current of DEU flows through the corresponding converter and wire resistance to supply power to the load. Compared with a mesh network, there is no complex coupling relationship between output currents. As mentioned earlier, the distributed loss of a single DEU is a quadratic function. The sum of them is the total loss, which is naturally a concave function. Given the balance of energy supply and consumption, this loss model is one concave function. Through the on-line adjustment of current coefficients, the loss of the distribution network can be accurately minimized.

Concave Optimization Algorithms

Inspired by the work on the concave optimization–based economical dispatch for generation cost minimization (Akbari-Dibavar et al., 2021), the concave optimization technique such as the dual ascent optimization method (DAOM) is applied in this work to solve the loss minimization problem. In recent years, the concave optimization algorithms, that is, Lagrange multiplier algorithm (Jiang et al., 2021c), dual decomposition algorithm (Jiang et al., 2021d), DAOM (Chen et al., 2017), and alternating direction method of multipliers (ADMM) (Chen and Yang, 2018) have attracted lots of attention for its wide implementations to solve problems in real systems, that is, parallel calculation, power dispatch, machine learning, and game theory. However, some practical problems for the implementation of power electronics should be considered. For example, the computation complexity of the applied algorithm should not affect the closed-loop PWM control of the MCU. By using a centralized data-exchange network, the Lagrange multiplier needs division operation and global data to obtain results (Jiang et al., 2021d), which reduces the scalability in large-scale AC microgrids. In the dual ascent algorithm, the division operation is necessary for current coefficient calculation. By adding a quadratic term of the constraint function, the convergence rate of ADMM is accelerated. However, such operation leads to an increase in computational complexity, which reduces its applicability in real-time high-frequency PWM control. For the DAOM, both Lagrange multiplier and current coefficients can be obtained through simple addition and subtraction iteration for implementation. Thereby, it is reasonable to select the DAOM for concave optimization.

Secondary Control

After obtaining the optimal current coefficient, the three-phase converter shall adopt an appropriate active and reactive power distribution strategy. So far, different strategies have been proposed. To achieve accurate power distribution, the droop scheme regulates the output voltage and frequency to compensate for the imbalance among output powers from DEUs (Sun et al., 2017), (Loh et al., 2013). In the study by Sun et al. (2017), the adaptive voltage term is introduced by using active sharing error to regulate the bus voltages. Moreover, this droop scheme is combined with an integrator for power quality improvement (Loh et al., 2013). When inductive reactance plays a leading role in the line, the virtual inductance is generated by the active power dispatch term for frequency regulation (Morstyn et al., 2018).

In the hybrid microgrid, the power balancing control is achieved by one proper-designed interconnection control scheme (Wu et al., 2018). A multi-agent–based power sharing control is used to allocate the power flow to enhance voltage quality (Yang et al., 2020). The voltage error and frequency control are used to regulate the power distribution and bus voltage simultaneously (Yao et al., 2011). Vijay et al. (2021) used the consensus algorithm to adaptively regulate the bus voltage of DEUs according to the measured values of DEU nodes so as to achieve realize bus voltage restoration. So far, relatively little work has been carried out in considering the power loss as the control parameter. Generally, for the scenarios of long-distance AC networks, the wire inductance is large. Thereby, the active power-frequency control is usually applied by considering the inductive impedance. According to the different types of wire, the modified droop strategy has been designed and implemented in the case of pure inductance (Jiang et al., 2021e; Keyvani-Boroujeni et al., 2021; Huang et al., 2022) and pure resistance impedance (Luo et al., 2022), but few research studies explore the complex impedance of the system. In applications, the distance between different converter units is a little far, and the inductance and resistance wire impedance cannot be ignored through the parallel connection of different wires. In addition, due to the possibility of multi-feedback design, the impedance of the power converter is actually very complex. Due to the coupling between the active and reactive power, traditional control cannot achieve efficient power sharing.

Contributions

As mentioned earlier, the distributed losses of one single DEU in the AC microgrid can be written as a quadratic function. As a combination, the total loss function of the AC microgrid can be obtained. As a multi-variable function, it is proven that the total loss is a concave function with respect to the current distribution coefficients. Furthermore, considering the supply-consumption balance, the proposed total loss model is an equality constrained concave function. In this work, the double ascent optimization method (DAOM) is designed to find the optimal current coefficient. By conducting the Lagrangian model, the optimal current coefficient can be iteratively calculated by the DAOM by simple addition and subtraction. In order to apply the current coefficient to the general PQ control structure, the calculation method of conversion between the current coefficient and power coefficient is designed. With the help of average reactive power, the active power distribution coefficients are obtained by using the voltages and currents of DEUs. For short-distance AC
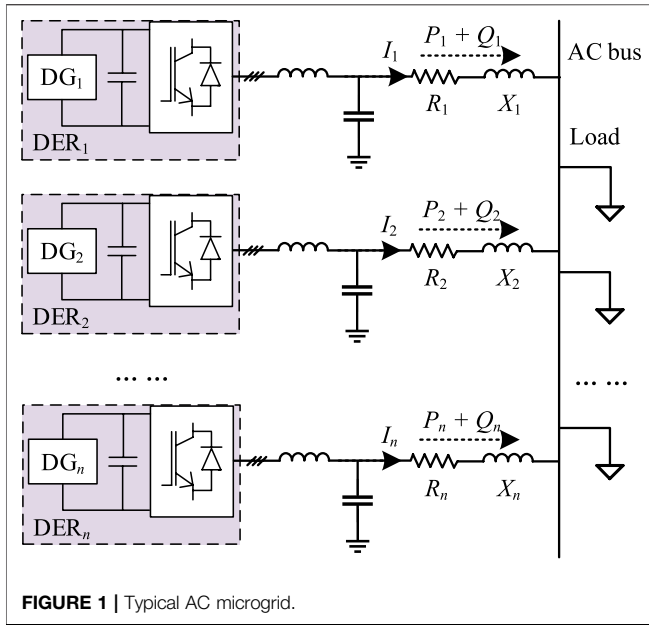
FIGURE 1 | Typical AC microgrid.

microgrids with a high resistance-to-reactance ratio (for example, R/X = 7.7), the conventional P-ω droop control and Q-E droop control are not suitable for power distribution among DEUs. In this work, an improved adaptive droop control strategy, composed of P-E droop control and Q-ω droop control, is proposed to dispatch the output active powers and reactive powers of DEUs. In this way, a multilayer control structure is proposed, including the DAOM in the top layer, P-E droop control and Q-ω droop control in the second layer, and voltage-current control in the lower layer. Simulation results verify the effectiveness of the proposed control strategy in reducing distribution losses.

AC MICROGRID CONFIGURATION AND LOSS MODELLING

Figure 1 shows the typical configuration of the autonomous AC microgrid. In the system, multiple distributed generation (DG) is integrated into one common bus. Power electronic devices such as inverters are generally used as they can provide flexible control of the DGs. To simplify the analysis, we assume that the DGs are all driven through voltage source inverters.

The power loss in an AC microgrid can be divided into two parts: converter loss P_{loss}^{conv} and wire loss P_{loss}^{line}. Although the power loss in a practical converter may also be affected by parasitic parameters and auxiliary circuits (e.g., protection circuits of the input current), the main power loss of converters is caused by the i) average conduction loss of switches, ii) average conduction loss by bypass diodes, iii) average switching loss, iv) reverse recovery loss in bypass diodes, and v) power loss on resistive elements in general operating conditions. The general mathematical expression of the main power loss in the converter is given as

$$P_{\text{loss}i}^{\text{conv}} = P_{\text{con}Si} + P_{\text{con}Di} + P_{\text{sw}i} + P_{\text{rec}i} + P_{\text{res}i}. \tag{1}$$

The average conduction loss power in diodes and switches (i.e., $P_{\text{con}Di}$ and $P_{\text{con}Si}$) can be given as

$$P_{\text{con}Si} = R_{\text{ON}i}I_{Ci\_\text{rms}}^2 + V_{\text{ON}i}I_{Ci\_\text{ave}}, \tag{2.1}$$

$$P_{\text{con}Di} = R_{\text{ON}i}I_{Fi\_\text{rms}}^2 + V_{\text{FO}i}I_{Fi\_\text{ave}}, \tag{2.2}$$

where $R_{\text{ON}i}$ is the ON-state resistance of the semiconductor devices of the ith converter. $V_{\text{ON}i}$ is the voltages across the semiconductor devices. $V_{\text{FO}i}$ is the forward voltages of the diodes. I_{Ci_ave}, I_{Fi_ave}, I_{Ci_rms}, and I_{Fi_rms} are the average and root mean square currents of the switches and diodes, respectively. For simplification, the average and root mean square currents of the semiconductor devices can be considered in linear relationships to the output currents of the grid-connected converters. Thus, the average conduction loss of diodes and switches can be expressed as

$$P_{\text{con}Si} = A_{1i}I_i^2 + A_{2i}I_i, \tag{3.1}$$

$$P_{\text{con}Di} = A_{3i}I_i^2 + A_{4i}I_i. \tag{3.2}$$

The average switching loss consists of the turn-on and turn-off loss, which can be calculated based on

$$P_{\text{sw}i} = P_{\text{on}i} + P_{\text{off}i} = \frac{1}{6}V_{\text{ON}i}I_{Ci\_\text{ave}}t_{\text{on}i}f_{\text{sw}i} + \frac{1}{6}V_{\text{ON}i}I_{Ci\_\text{ave}}t_{\text{off}i}f_{\text{sw}i}, \tag{4}$$

where $t_{\text{on}i}$ and $t_{\text{off}i}$ are the turn-on and turn-off time, respectively. $f_{\text{sw}i}$ is the switching frequency. For simplification, the conduction currents can be considered in linear relationships to the output currents of the converters. Therefore, the average switching loss can be expressed as

$$P_{\text{sw}i} = A_{5i}I_i. \tag{5}$$

The reverse recovery loss power of bypass diodes can be calculated based on

$$P_{\text{rec}i} = V_{gi}I_{Fi\_\text{ave}}t_{ri}f_{\text{sw}i} + V_{gi}Q_{rri}f_{\text{sw}i}, \tag{6}$$

where V_{gi} is the dc-link voltage of the ith grid-connected converter. t_{ri} is the reverse-recovery time. Q_{rri} is the reverse recovery charge of the diodes in the ith grid-connected converter. In a system-level analysis, the average switching loss can be expressed as

$$P_{\text{rec}i} = A_{6i}I_i + A_{7i}. \tag{7}$$

In addition, the power loss on resistive elements can be calculated based on

$$P_{\text{res}i} = R_{\text{re}}I_i^2, \tag{8}$$

where R_{re} is the equivalent resistance of the converter.

As given in (**1–8**), the total power loss of the converter in the DEU system can be expressed as follows

$$P_{loss}^{conv} = P_{\text{con}S} + P_{\text{con}D} + P_{\text{sw}} + P_{\text{rec}} + P_{\text{res}}. \tag{9}$$

As proposed in the study by Fooladivanda et al. (2021) and Beerten et al. (2012) and the aforementioned analysis, by defining the loss coefficients as a_i, b_i, and c_i, the converter loss is written as
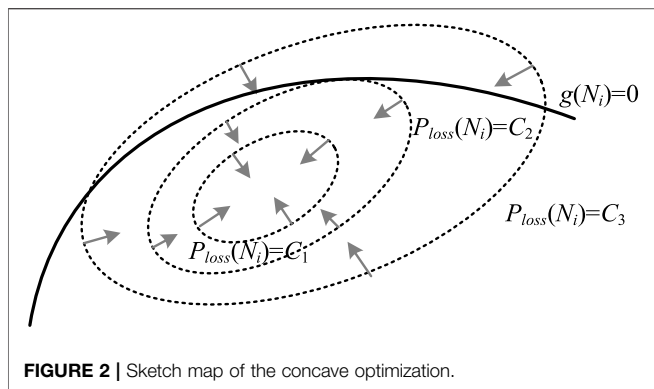
FIGURE 2 | Sketch map of the concave optimization.

$$P_{lossi}^{conv} = a_i I_i^2 + b_i |I_i| + c_i. \tag{10}$$

In addition, by adding the wire loss, the total loss is written as

$$P_{lossi} = P_{lossi}^{conv} + P_{lossi}^{line} = R_i I_i^2 + a_i I_i^2 + b_i |I_i| + c_i, \tag{11}$$

where R_i is the equivalent wire resistance. Based on **(11)**, the loss of the AC microgrid is given as

$$P_{loss}(N_i) = \sum_{i=1}^{n} P_{lossi} = \sum_{i=1}^{n} \left[(R_i + a_i)(N_i I_{tol})^2 + b_i |N_i I_{tol}| + c_i \right], \tag{12.1}$$

$$I_{tol} = \sum_{i=1}^{n} I_i, \tag{12.2}$$

where N_i is the current distribution coefficient of DEU_i, $N_i I_{tol} = I_i$, and I_{tol} is the total load currents. Thus, one equality constraint can be obtained as

$$\sum_{i=1}^{n} I_i = \sum_{i=1}^{n} N_i I_{tol} = I_{tol} \Rightarrow g(N_i) = \sum_{i=1}^{n} N_i - 1 = 0. \tag{13}$$

To reveal the concave characteristic of the loss function, its first-order derivative and second-order derivative are given as

$$\partial P_{loss}(N_i) / \partial N_i = 2N_i (I_{tol})^2 (R_i + a_i) + b_i |I_{tol}| \ge 0, \tag{14.1}$$

$$\partial^2 P_{loss}(N_i) / \partial N_i^2 = 2(I_{tol})^2 (R_i + a_i) \ge 0. \tag{14.2}$$

As proven in (14), the loss function is strictly concave. In this work, the cost function to be optimized is given as

$$\begin{aligned} \text{minimize} \quad & J = P_{loss}(N_i), \\ \text{subject to} \quad & \sum_{i=1}^{n} (N_i) = 1, \\ & P_{\min i} \le P_i \le P_{\max i}, \end{aligned} \tag{15}$$

where $P_{\min i}$ and $P_{\max i}$ are the output power limits.

CONTROL STRATEGY FOR LOSS MINIMIZATION
DAOM for Current Distribution Coefficients Optimization

As presented in **Figure 2**, the sketch map of the concave function is presented, where the concave function $P_{loss}(N_i)$ can be seen

graphically. Here, the one concave optimization algorithm DAOM is selected for iterative optimization.

Based on **(15)**, an augmented Lagrange function is defined as

$$L_{\rho i}(N_i, \lambda) = (a_i + R_i)(N_i I_{tol})^2 + b_i N_i |I_{tol}| + c_i + \lambda \left(\sum_{i=1}^{n} N_i - 1 \right)$$
$$+ \frac{\rho}{2} \left(\sum_{i=1}^{n} N_i - 1 \right)^2, \tag{16}$$

where λ is the Lagrange multiplier and $\lambda \ne 0$, ρ is a coefficient. As given in the study by Jiang et al. (2021d) and Boyd and Vandenberghe (2004), all calculations for λ and optimal current allocation coefficients are completed in the central controller. With a large number of DEUs, the heavy calculation burden affects the scalability of the given Lagrange multiplier method. Instead of solving the function directly, the DAOM is proposed as an iterative optimization. The idea is to start at an initial guess, take a small step in the direction of the gradient, and repeat. Specifically, we use gradient ascent on the dual variables. The current coefficients can be updated as follows:

$$N_i^{k+1} = \arg \min L(N_i^k, \lambda^k). \tag{17}$$

The following equation should be satisfied as

$$\nabla_{N_i, \lambda} L(N_i^k, \lambda^k) = \left(\frac{\partial L}{\partial N_i^k}, \frac{\partial L}{\partial \lambda^k} \right) = 0 \tag{18}$$

which yields

$$N_i^{k+1} = -\frac{b_i |I_{tol}| + \lambda^k + \rho \left(\sum_{i=1}^{n} N_i^k - 1 \right)}{2(a_i + R_i)(I_t)^2}. \tag{19}$$

Updating λ based on the residual of the linear constraint, the update rule in the central controller for λ can be expressed as follows:

$$\lambda^{k+1} = \lambda^k + \alpha \left(\sum_{i=1}^{n} N_i^{k+1} - 1 \right), \tag{20}$$

where α is a coefficient. The main advantage of the DAOM is the parallel execution of N_i updates. It is noteworthy that this inequality constraint will not change the convexity of the proposed loss model. Due to inequality constraints, some current coefficients will be set to constant values. Interestingly, the new loss function formed by the remaining DEUs is still a concave function with respect to the remaining N_i. Thereby, the DAOM can still be used for optimization.

P-E Droop Control and Q-ω Droop Control

As designed earlier, the current coefficient is obtained for loss minimization. Given the generally used PQ control structure, the current coefficient cannot be applied directly in the AC microgrid. Therefore, the current coefficient should be converged to the power distribution variables for power dispatch. Hence, the relationship between the output current and output power in a DEU is discussed for further control development. In an AC microgrid, the injection

TABLE 1 | Injected powers under different types of impedances.

Types of impedance	Pure inductance $Z_i = jX_i$	Pure resistance $Z_i = R_i$	Complex impedance $Z_i = R_i + jX_i$
Active power	$P_i \approx \frac{V_{bus}E_i\phi_i}{Z_i}$	$P_i \approx \frac{V_{bus}E_i}{R_i} - \frac{V_{bus}^2}{R_i}$	$P_i \approx \frac{V_{bus}}{Z_i}[(E_i - V_{bus})\cos\theta_i + E_i\phi_i\sin\theta_i]$
Reactive power	$Q_i \approx \frac{V_{bus}(E_j - V_{bus})}{Z_i}$	$Q_i \approx -\frac{V_{bus}E_i}{R_i}\phi_i$	$Q_i \approx \frac{V_{bus}}{Z_i}[(E_i - V_{bus})\sin\theta_i + -E_i\phi_i\cos\theta_i]$
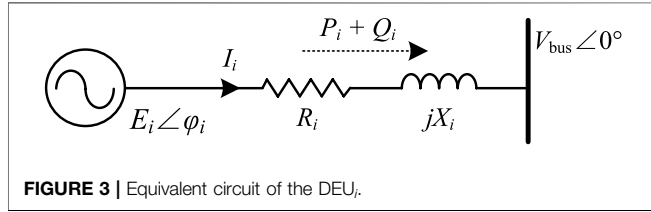
FIGURE 3 | Equivalent circuit of the DEU$_i$.

power is determined by the ratio of resistance and inductive reactance in the wire. As summarized in **Table 1**, in a short-distance AC microgrid, the injection active power is determined by the voltage amplitude of the DEU, and the injection reactive power is determined by the frequency of the DEU. The equivalent circuit of DEU$_i$ is plotted in **Figure 3**: $Z_i = R_i + jX_i$ is the wire impedance, θ_i is the wire impedance angle, $E_i \angle \varphi_i$ is the terminal electromotive force of the converter, and $V_{bus} \angle 0^\circ$ is the voltage of the common AC bus.

As given in **Table 1**, the injection power by DEU$_i$ is given as

$$P_i \approx \frac{V_{bus}E_i}{R_i} - \frac{V_{bus}^2}{R_i}, \quad Q_i \approx -\frac{V_{bus}E_i}{R_i}\phi_i, \quad (21)$$

As given in (**21**), the output active power of the converter is positively correlated with the amplitude of the terminal electromotive force. The output reactive power of the converter is negatively correlated with the operating frequency of the converter. In this way, one droop control is designed as

$$E_{refi} = E_{nom} - m_iP_i, \quad m_i = (E_{max} - E_{min})/P_{maxi}, \quad (22.1)$$

$$\omega_{refi} = \omega_{nom} + n_iQ_i, \quad n_i = (\omega_{max} - \omega_{min})/Q_{maxi}, \quad (22.2)$$

where ω_{refi} and ω_{nom} are the reference value and nominal value of angle frequency, respectively, and E_{refi} and E_{nom} are the reference value and nominal value of angle frequency voltage amplitude, respectively. Meanwhile, the limits of angle frequency and voltage amplitude are also considered in (**22**): m_i and n_i are the droop coefficients, Q_{maxi} is the reactive power limit of the DEU$_i$, ω_{min} and E_{min} are the minimum values of angle frequency and voltage amplitude, and ω_{max} and E_{max} are the maximum values of angle frequency and voltage amplitude, respectively. According to the apparent power, the output current of the DEU$_i$ is

$$I_i = \sqrt{2}\sqrt{P_i^2 + Q_i^2}/E_i = \sqrt{P_i^2 + Q_i^2}/V_i, \quad (23)$$

where V_i is RMS values of voltage $E_i \angle \varphi_i$. Based on (**23**), it yields

$$(V_i)^2(N_iI_{tol})^2 = (N_{Pi}P_{tol})^2 + (N_{Qi}Q_{tol})^2, \quad (24.1)$$

where P_{tol} and Q_{tol} are the total demanding powers. N_{Pi} and N_{Qi} are defined as the active power and reactive power coefficients of

DEU$_i$, respectively. Thus, the average reactive power distribution is adopted as

$$N_{Qi} = 1/n. \quad (24.2)$$

Given the power generation limitation, the active power can be dispatched as

$$N_{Pi} = \begin{cases} P_{mini}/P_{tol} & P_i < P_{mini} \\ P_{maxi}/P_{tol} & P_i > P_{maxi} \\ \sqrt{(V_i)^2(N_iI_{tol})^2 - (Q_{tol}/n)^2}/P_{tol} & \text{others} \end{cases} \quad (24.3)$$

Moreover, a secondary adaptive control layer is implemented as

$$e_{Pi} = -\sum_{i \neq j}^{n}(x_{Pi} - x_{Pj}), e_{Qi} = -\sum_{i \neq j}^{n}(x_{Qi} - x_{Qj}), \quad (25)$$

where $x_{Pi} = P_i/N_{Pi}$ and $x_{Qi} = Q_i/N_{Qi}$. x_{Pi} and x_{Qi} are defined as the inter-media variables for power distribution. Then, the adaptive voltage and frequency terms are generated as

$$E_{adpi} = (k_{EPi} + k_{EIi}/s)e_{Pi}, \omega_{adpi} = (k_{\omega Pi} + k_{\omega Ii}/s)e_{Qi}, \quad (26)$$

where k_{Epi}, k_{EIi}, $k_{\omega Pi}$, and $k_{\omega Ii}$ are the gains of controllers. Thus, the secondary control is formed as

$$E_{refi} = E_{nom} - m_iP_i - E_{adpi}, \omega_{refi} = \omega_{nom} + n_iQ_i + \omega_{adpi}. \quad (27)$$

As plotted in **Figure 4**, the proposed P-E and Q-ω control are presented in (a), and the diagram is given in (b). Based on the concave loss model, the optimal current distribution coefficients of each inverter are computed according to the DAOM. By using average reactive power sharing, the active power distribution coefficients are calculated. In addition, the output power of each DEU is calculated locally. Then, these coefficients are incorporated into the local droop controller to perform optimum power sharing. The reference values of angle frequency and voltage amplitude by adaptive droop control are further used for local voltage and current closed-loop control. In this way, the concave optimization–based current and power sharing for distribution loss minimization is achieved.

CASE STUDIES

The simulation-based case study is conducted in MATLAB/Simulink with four DEU systems. The main parameters of the AC microgrid are shown in **Table 2**. In this work, the loads are considered current sinks whose current. The allowable voltage deviations are $V_{min} = 209$ V and $V_{max} = 231$ V. The rated power of the four DEU systems is given as 4 kW. The algorithm execution
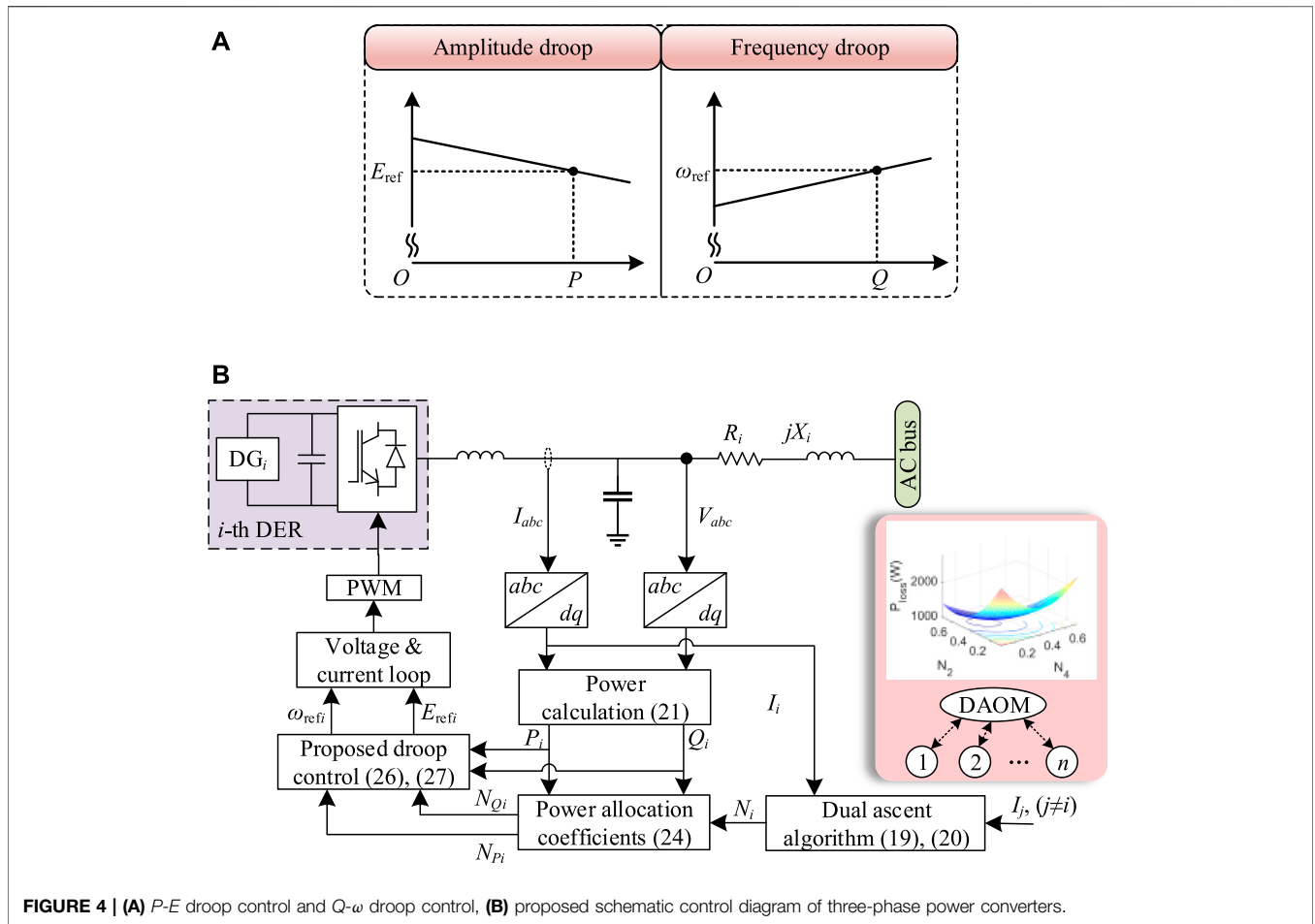
FIGURE 4 | **(A)** *P-E* droop control and *Q-ω* droop control, **(B)** proposed schematic control diagram of three-phase power converters.

TABLE 2 | Parameters of AC microgrids.

Parameters	Value
Nominal electromotive force (E_{nom})	220 $\sqrt{2}$V
Nominal angle frequency (ω_{nom})	100 π rad/s
Total load (S)	9.65 kW + 3.76 kVar
Generation capacity (P_{maxi})	4 kW
Wire impedance of DEU1 (R1 + jX1)	0.963 + j0.125 Ω
Wire impedance of DEU2 (R2 + jX2)	2.568 + j0.334 Ω
Wire impedance of DEU3 (R3 + jX3)	1.926 + j0.250 Ω
Wire impedance of DEU4 (R4 + jX4)	1.284 + j0.167 Ω

TABLE 3 | Converter loss coefficients.

Converter number	a_i	b_i	c_i
1	1.162	2.960	12.14
2	0.577	1.250	32.14
3	0.277	0.956	44.36
4	1.430	1.403	20.61

period of the DAOM is set to 1s. The PWM frequency and the sampling frequency of the local closed-loop control are 10 kHz. For DEU systems 1, 2, 3, and 4, the converter loss coefficients are presented in **Table 3**.

Convexity Verification of the Distribution Loss Model

The convexity of the loss model is preliminarily verified by the exhaustive search method in the simulation model. By fixing the change step of the current coefficient, the new coefficient is

continuously brought into the AC microgrid to obtain the loss value. For example, the DEU2 and DEU3 are selected to form an AC microgrid. Then, the distribution losses with respect to current coefficients under different load currents (8, 12, 16, and 20 A) are plotted in **Figure 5A**. The loss curves of another AC microgrid with DEU1 and DEU4 are also presented in **Figure 5B**. Due to the equality constraint, only one coefficient can be adjusted for an AC microgrid in the case of two DEUs. As can be seen, both eight curves in **Figure 5** are conic with one minimum point.

Furthermore, two current coefficients can be regulated in the searching process for the three DEU-based AC microgrid under 30 A load current. Therefore, the system loss can be drawn as a three-dimensional surface. As given in **Figure 6**, four loss surfaces correspond to four different DEU combinations: DEU$_1$, DEU$_2$,

FIGURE 5 | AC microgrid loss with two DEUs. **(A)** DEU_2 and DEU_3, **(B)** DEU_1 and DEU_4.

FIGURE 6 | Loss with three DEU systems. **(A)** DEU_1, DEU_2, and DEU_3, **(B)** DEU_1, DEU_2, and DEU_4, **(C)** DEU_1, DEU_3, and DEU_4, **(D)** DEU_2, DEU_3, and DEU_4.

FIGURE 7 | Distribution loss with respect to current coefficients for fixed **(A)** N_1, **(B)** N_2, **(C)** N_3, and **(D)** N_4.
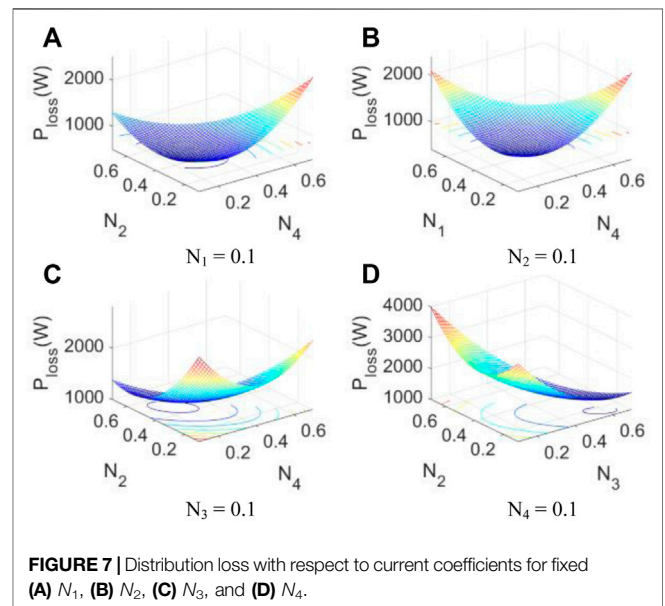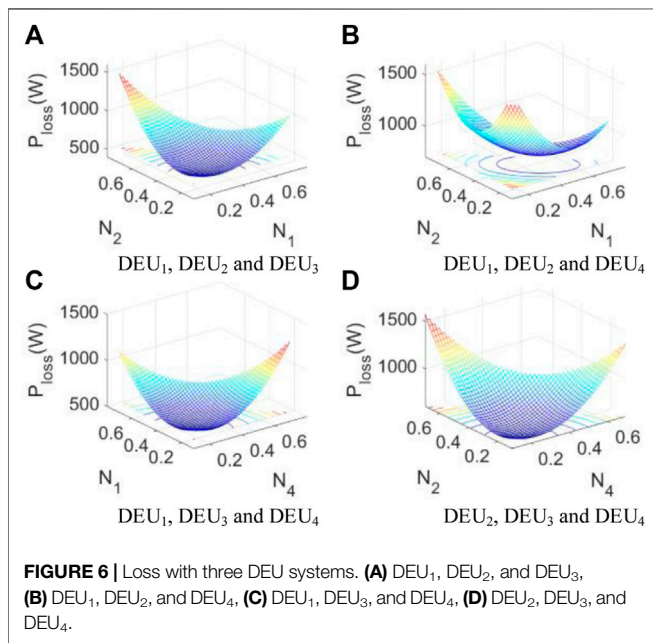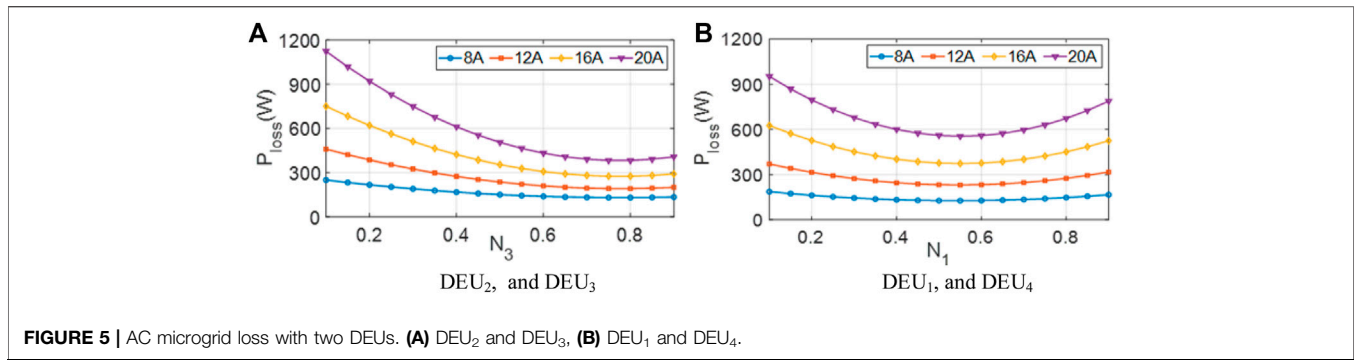
and DEU_3 in **Figure 6A**, DEU_1, DEU_2, and DEU_4 in **Figure 6B**, DEU_1, DEU_3, and DEU_4 in **Figure 6C**, and DEU_2, DEU_3, and DEU_4 in **Figure 6D**). The contours of the losses are also projected onto the bottom surface. Apparently, both surfaces with openings upward are smooth, which are the typical concave surfaces.

For the system with four DEUs, the loss surface cannot be plotted directly with three adjustable variables. Therefore, we can fix the current coefficient value of one DEU so as the loss model degenerates into a three-dimensional surface. The total load current is 48 A. By fixing the one current coefficient at 0.1 in turn, four three-dimensional loss surfaces are obtained in **Figure 7**. Obviously, both surfaces with an opening upward are smooth, which are typical concave functions. For an AC microgrid with more DEUs, the convexity of the proposed loss model cannot be graphically illustrated. However, as shown in the previous figures, the theoretical proof has been provided in **Section 2**

Case 1: Normal Operation
Optimal control studies by the proposed DAOM and the *P-E* and *Q-ω* control are also presented based on the aforementioned

analyzed AC distribution network. In case 1, the traditional control and the proposed control are adopted for the four DEUs in the periods from 0 to 3 s and 3–32 s, respectively. **Figure 8** shows the waveforms of the voltages, output currents, current distribution coefficients, active powers, active power allocation coefficients, reactive powers, reactive power allocation coefficients for the DEUs in the AC microgrid, and the loss. At the initial condition, the current coefficients of DEUs are $N_1 = 0.33$, $N_2 = 0.18$, $N_3 = 0.21$, and $N_4 = 0.28$, and the output active power allocation coefficients of DEUs are $N_{P1} = 0.34$, $N_{P2} = 0.17$, $N_{P3} = 0.21$, and $N_{P4} = 0.28$. The output powers are $P_1 = 3.3$ kW, $P_2 = 1.6$ kW, $P_3 = 2.0$ kW, and $P_4 = 2.75$ kW and $Q_1 = Q_2 = Q_3 = Q_4 = 0.94$ kVar. These output power and current allocation rates are determined by the different wire impedances and voltage for DEUs. Meanwhile, b uses the converter loss coefficients and wire resistances in **Tables 2** and **3**, and the loss is calculated as 1097 W (converter loss is 812 W, and the wire loss is 285 W).

When the proposed DAOM is applied at 3 s, the current distribution coefficients, active power allocation coefficients, and reactive power allocation coefficients are continuously updated in a cycle of 1 s. At the same time, the distributed
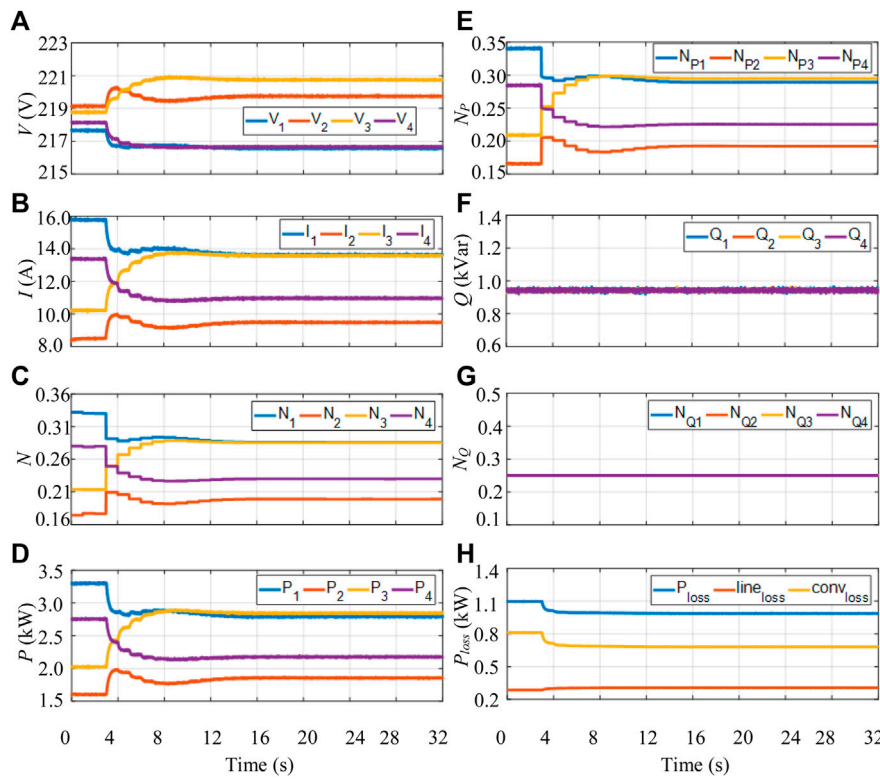
FIGURE 8 | **(A)** Voltages, **(B)** output currents, **(C)** current distribution coefficients, **(D)** active powers, **(E)** active power allocation coefficients, **(F)** reactive powers, **(G)** reactive power allocation coefficients, and **(H)** power loss.

TABLE 4 | Control results of case 1.

Current distribution coefficients	Initial value	Optimal value	Active power allocation coefficients	Initial value	Optimal value
N_1	0.33	0.29	NP1	0.34	0.29
N_2	0.18	0.20	NP2	0.17	0.19
N_3	0.21	0.28	NP3	0.21	0.29
N_4	0.28	0.23	NP4	0.28	0.23

secondary control regulates the output active powers and reactive powers according to the updating power ratio. After iteration, the current distribution coefficients are optimized at $N_1^* = 0.29$, $N_2^* = 0.20$, $N_3^* = 0.28$, and $N_4^* = 0.23$ at steady state. The results are coincided with the minimum point of the proposed loss model by the concave optimization theory. With the help of $N_{Qi} = 0.25$, the optimal active power allocation coefficients are obtained as $N_{P1}^* = 0.29$, $N_{P2}^* = 0.19$, $N_{P3}^* = 0.29$, and $N_{P4}^* = 0.23$. Then, the output powers from DEUs are distributed as 2.8, 1.85, 2.83, and 2.17 kW by the designed P-E and Q-ω droop controls. By using the aforementioned parameters, the coefficient updating process of the DAOM is smooth, with the well regulation of output currents. The corresponding wire loss, converter loss, and distribution loss by the designed control are 306 W, 680 W,

and 986 W, respectively. By comparing with the conventional method, the wire loss is increased by 21 W, while the converter loss is decreased by 132 W. Therefore, the total distribution power loss of the proposed control is reduced by 111 W (reduced by 10.12%). Furthermore, the output powers and bus voltages of DEUs are controlled within the limitations during the whole control process. The final convergence values of current coefficients and active power coefficients are presented in **Table 4**. These values are consistent with the theoretical minimum point of the loss model. Therefore, both DAOM P-E droop control and Q-ω droop control are proven.

Case 2: Wire Resistance Variation

In case 2, the study on the variation of wire resistance is carried out: R_3 is revised as 0.214 Ω (Pecht et al., 2017; Zhang et al., 2019;
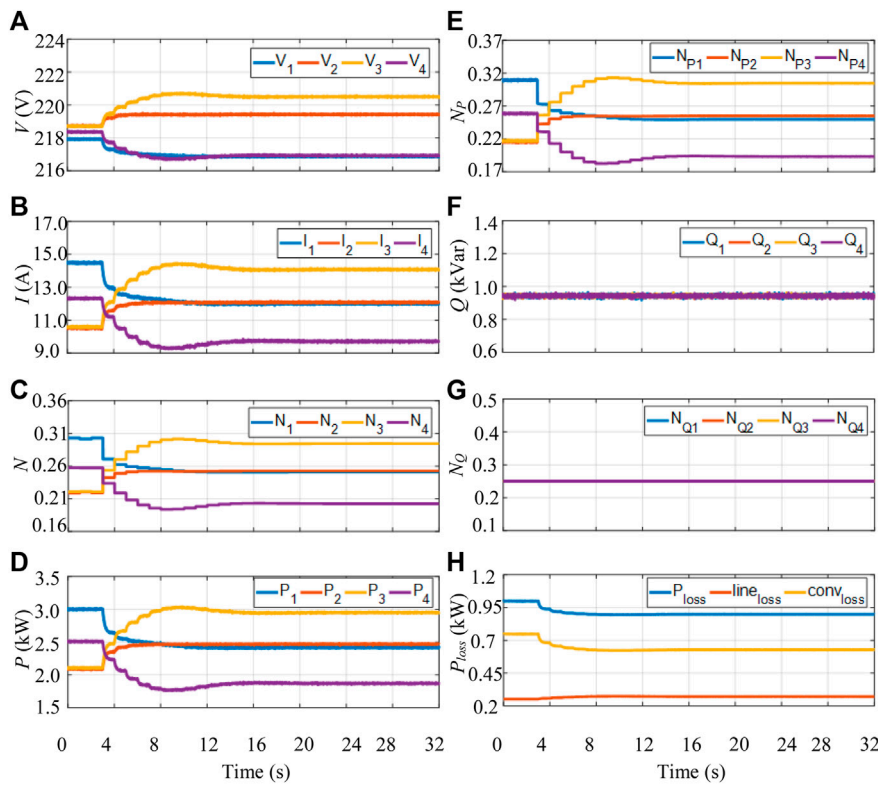
FIGURE 9 | (A) Voltages, **(B)** output currents, **(C)** current distribution coefficients, **(D)** active powers, **(E)** active power allocation coefficients, **(F)** reactive powers, **(G)** reactive power allocation coefficients, and **(H)** power loss.

TABLE 5 | Control results of case 2.

Current distribution coefficients	Initial value	Optimal value	Active power allocation coefficients	Initial value	Optimal value
N_1	0.30	0.25	NP1	0.31	0.250
N_2	0.22	0.25	NP2	0.21	0.255
N_3	0.22	0.30	NP3	0.22	0.305
N_4	0.26	0.20	NP4	0.26	0.190
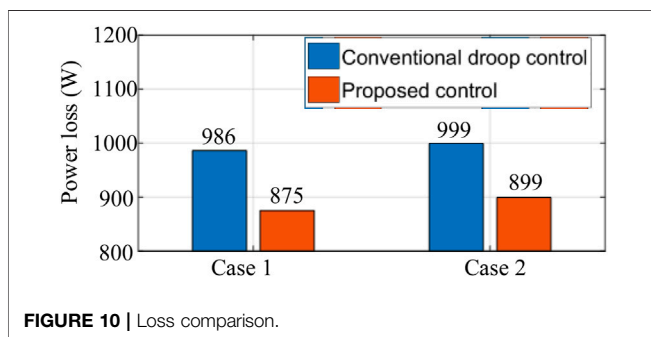
FIGURE 10 | Loss comparison.

Singh et al., 2020). **Figure 9** shows the control results of the voltages, output currents, current allocation coefficients, active powers, active power allocation coefficients, reactive powers,

reactive power allocation coefficients for the DEUs, and the loss. At the initial condition, the current coefficients of DEUs are $N_1 = 0.30$, $N_2 = 0.22$, $N_3 = 0.22$, and $N_4 = 0.26$ and the output active power allocation coefficients of DEUs are $N_{P1} = 0.30$, $N_{P2} = 0.21$, $N_{P3} = 0.22$, and $N_{P4} = 0.26$. The output powers are $P_1 = 2.9$ kW, $P_2 = 2.05$ kW, $P_3 = 2.05$ kW, and $P_4 = 2.65$ kW and $Q_1 = Q_2 = Q_3 = Q_4 = 0.94$ kVar. These output power and current allocation rates are determined by the different wire impedances and voltage for DEUs. Meanwhile, b using the converter loss coefficients and wire resistances in **Tables 2** and **3**, the loss is calculated as 999 W (the converter loss is 748 W, and the wire loss is 251 W).

When the proposed DAOM is applied at 3 s, the current distribution coefficients, active power allocation coefficients, and reactive power allocation coefficients are continuously updated in a cycle of 1 s. At the same time, the distributed secondary control regulates the output active powers and

reactive powers according to the updating power ratio. After iteration, the current distribution coefficients are optimized at $N_1^* = 0.25$, $N_2^* = 0.25$ $N_3^* = 0.30$ and $N_4^* = 0.20$ at steady state. The results are coincided with the minimum point of the proposed loss model by the concave optimization theory. With the help of $N_{Qi} = 0.25$, the optimal active power allocation coefficients are obtained as $N_{P1}^* = 0.250$, $N_{P2}^* = 0.255$, $N_{P3}^* = 0.305$, and $N_{P4}^* = 0.190$. Then, the output powers from DEUs are distributed as 2.40, 2.46, 2.94, and 1.85 kW by the designed $P\text{-}E$ and $Q\text{-}\omega$ droop control. By using the aforementioned parameters, the coefficient updating process of the DAOM is smooth, with the well regulation of output currents. The corresponding wire loss, converter loss, and distribution loss by designed control are 271, 628, and 899 W, respectively. By comparing with the conventional method, the wire loss is increased by 20 W, while the converter loss is decreased by 120 W. Therefore, the total loss of the proposed control is reduced by 100 W (reduced by 10.01%). Moreover, the bus voltages and output powers of DEUs in **Figure 9** are regulated within the limitations. The iteration results by the DAOM of case 2 are given in **Table 5**. The optimal values of the current and active power allocation coefficients coincide with the theoretical analysis.

Figure 10 shows the loss comparison. Compared with the traditional method, this control scheme reduces the power loss of the distribution network by about 10.12 and 10.01% in case 1 and case 2, respectively.

REFERENCES

Akbari-Dibavar, A., Mohammadi-Ivatloo, B., Zare, K., Khalili, T., and Bidram, A. (2021). Economic-emission Dispatch Problem in Power Systems with Carbon Capture Power Plants. *IEEE Trans. Ind. Appl.* 57 (4), 3341–3351. doi:10.1109/tia.2021.3079329

Beerten, J., Cole, S., and Belmans, R. (2012). Generalized Steady-State VSC MTDC Model for Sequential AC/DC Power Flow Algorithms. *IEEE Trans. Power Syst.* 27 (2), 821–829. doi:10.1109/tpwrs.2011.2177867

Boyd, S., and Vandenberghe, L. (2004). *Convex Optimization*. Cambridge, U.K.: Cambridge Univ. Press.

Chen, G., Li, C., and Dong, Z. (2017). Parallel and Distributed Computation for Dynamical Economic Dispatch. *IEEE Trans. Smart Grid* 8 (2), 1026–1027. doi:10.1109/TSG.2016.2623980

Chen, G., and Yang, Q. (2018). An ADMM-Based Distributed Algorithm for Economic Dispatch in Islanded Microgrids. *IEEE Trans. Ind. Inf.* 14 (9), 3892–3903. doi:10.1109/tii.2017.2785366

Fooladivanda, D., Hu, Q., and Chang, Y. H. (2021). Secure Dynamic State Estimation for Cyber Security of AC Microgrids. *Front. Control. Eng.* 2, 734220. doi:10.3389/fcteg.2021.734220

Huang, W., Shuai, Z., Shen, X., Li, Y., and Shen, Z. J. (2022). Dynamical Reconfigurable Master–Slave Control Architecture (DRMSCA) for Voltage Regulation in Islanded Microgrids. *IEEE Trans. Power Electron.* 37 (1), 249–263. doi:10.1109/TPEL.2021.3086192

Jiang, Y., Yang, Y., Tan, S.-C., and Hui, S.-Y. R. (2021). Distribution Power Loss Mitigation of Parallel-Connected Distributed Energy Resources in Low-Voltage DC Microgrids Using a Lagrange Multiplier-Based Adaptive Droop Control. *IEEE Trans. Power Electron.* 36 (8), 9105–9118. doi:10.1109/tpel.2021.3050506

Jiang, Y., Yang, Y., Tan, S.-C., and Hui, S. Y. (2021). Distributed Sliding Mode Observer-Based Secondary Control for DC Microgrids under Cyber-Attacks. *IEEE J. Emerg. Sel. Top. Circuits Syst.* 11 (1), 144–154. doi:10.1109/jetcas.2020.3046781

Jiang, Y., Yang, Y., Tan, S. C., and Hui, S. Y. R. (2021). A High-Order Dixfferentiator Based Distributed Secondary Control for Dc Microgrids against False Data Injection Attacks. *IEEE Trans. Smart Grid.* early access. doi:10.1109/TSG.2021.3135904

Jiang, Y., Yang, Y., Tan, S. C., and Hui, S. Y. R. (2021). "Lagrange Multiplier-Based Optimization Control for Distribution Power Loss Minimization of Islanded Three-phase AC Microgrids," in *2021 IEEE/IAS Industrial and Commercial Power System Asia* (Chengdu, China: I&CPS Asia), 489–494. doi:10.1109/icpsasia52756.2021.9621641

Jiang, Y., Yang, Y., Tan, S. C., and Hui, S. Y. R. (2021). "Power Loss Mitigation of Parallel-Connected Distributed Energy Resources in DC Microgrids Using a Dual-Ascent Hierarchical Control," in *Proc. 2021 IEEE IAS Industrial & Commercial Power System Asia*, Chengdu, China, 18-21 July 2021. doi:10.1109/icpsasia52756.2021.9621706

Keyvani-Boroujeni, B., Fani, B., Shahgholian, G., and Alhelou, H. H. (2021). Virtual Impedance-Based Droop Control Scheme to Avoid Power Quality and Stability Problems in VSI-Dominated Microgrids. *IEEE Access* 9, 144999–145011. doi:10.1109/access.2021.3122800

Li, B., and Roche, R. (2021). Real-Time Dispatching Performance Improvement of Multiple Multi-Energy Supply Microgrids Using Neural Network Based Approximate Dynamic Programming. *Front. Electron.* 1. doi:10.3389/felec.2021.637736

Loh, P. C., Li, D., Chai, Y. K., and Blaabjerg, F. (2013). Autonomous Control of Interlinking Converter with Energy Storage in Hybrid AC–DC Microgrid. *IEEE Trans. Ind. Appl.* 49 (3), 1374–1382. doi:10.1109/TIA.2013.2252319

Luo, S., Wu, W., Koutroulis, E., Chung, H. S. H., and Blaabjerg, F. (2022). A New Kalman-Filter-Based Harmonic Current Suppression Method for the Virtual Oscillator Controlled Grid-Tied Inverter. *IEEE, J. Emer. Sel. Top. Circuits Syst.* 12 (1). doi:10.1109/jetcas.2022.3141106

Morstyn, T., Hredzak, B., and Agelidis, V. G. (2018). Network Topology Independent Multi-Agent Dynamic Optimal Power Flow for Microgrids with Distributed Energy Storage Systems. *IEEE Trans. Smart Grid* 9 (4), 3419–3429. doi:10.1109/tsg.2016.2631600

CONCLUSION

The wire loss and converter loss in the AC microgrid are modeled as a function of the current distribution coefficient. As analyzed, the loss model is a concave function with constraints. By applying the DAOM, the optimal current coefficients for DEUs are obtained by iteration. Then, according to the wire impedance in a short-distance AC microgrid, the novel $P\text{-}E$ droop control and $Q\text{-}\omega$ droop control are proposed to dispatch the output active powers and reactive powers of DEUs. Hence, real-time loss minimization control is achieved. Case studies are provided to verify the convexity of the proposed model and the effectiveness of the control strategy.

DATA AVAILABILITY STATEMENT

The original contributions presented in the study are included in the article/Supplementary Material; further inquiries can be directed to the corresponding author.

AUTHOR CONTRIBUTIONS

All authors listed have made a substantial, direct, and intellectual contribution to the work and approved it for publication.

Pecht, M. G., Agarwal, R., McCluskey, P., Dishongh, T., Javadpour, S., and Mahajan, R. (2017). *Electronic Packaging: Materials and Their Properties.* Boca Raton, FL: CRC Press.

Qian, X., Yang, Y., Li, C., and Tan, S.-C. (2020). Operating Cost Reduction of DC Microgrids under Real-Time Pricing Using Adaptive Differential Evolution Algorithm. *IEEE Access* 8, 169247–169258. doi:10.1109/access.2020.3024112

Singh, R. S., Cobben, S., and Ćuk, V. (2020). PMU-based Cable Temperature Monitoring and Thermal Assessment for Dynamic Line Rating. *IEEE Trans. Power Del.* 36 (3), 1859–1868. doi:10.1109/TPWRD.2020.3016717

Sun, Y., Hou, X., Yang, J., Han, H., Su, M., and Guerrero, J. M. (2017). New Perspectives on Droop Control in AC Microgrid. *IEEE Trans. Ind. Electron.* 64 (7), 5741–5745. doi:10.1109/tie.2017.2677328

Teng, J. H., Liao, S.-H., Huang, W.-H., and Chiang, C. C. (2016). Smart Control Strategy for Conversion Efficiency Enhancement of Parallel Inverters at Light Loads. *IEEE Trans. Ind. Electron.* 63 (12), 7586–7596.

Vijay, A. S., Parth, N., Doolla, S., and Chandorkar, M. C. (2021). An Adaptive Virtual Impedance Control for Improving Power Sharing Among Inverters in Islanded AC Microgrids. *IEEE Trans. Smart Grid* 12 (4), 2991–3003. doi:10.1109/tsg.2021.3062391

Wang, H., Khambadkone, A. M., and Yu, X. (2010). Control of Parallel Connected Power Converters for Low Voltage Microgrid-Part II: Dynamic Electrothermal Modeling. *IEEE Trans. Power Electron.* 25 (12), 2971–2980. doi:10.1109/tpel.2010.2087394

Wu, X., Shen, C., and Iravani, R. (2018). A Distributed, Cooperative Frequency and Voltage Control for Microgrids. *IEEE Trans. Smart Grid* 9 (4), 2764–2776. doi:10.1109/tsg.2016.2619486

Yang, Y., Qin, Y., Tan, S.-C., and Hui, S. Y. R. (2019). Efficient Improvement of Photovoltaic-Battery Systems in Standalone DC Microgrids Using a Local Hierarchical Control for the Battery System. *IEEE Trans. Power Electron.* 34 (11), 10796–10807. doi:10.1109/tpel.2019.2900147

Yang, Y., Qin, Y., Tan, S.-C., and Hui, S. Y. R. (2020). Reducing Distribution Power Loss of Islanded AC Microgrids Using Distributed Electric Springs with

Predictive Control. *IEEE Trans. Ind. Electron.* 67 (10), 9001–9011. doi:10.1109/tie.2020.2972450

Yao, W., Chen, M., Matas, J., Guerrero, J. M., and Qian, Z.-M. (2011). Design and Analysis of the Droop Control Method for Parallel Inverters Considering the Impact of the Complex Impedance on the Power Sharing. *IEEE Trans. Ind. Electron.* 58 (2), 576–588. doi:10.1109/tie.2010.2046001

Yuan, W., Wang, Y., and Chen, Z. (2021). New Perspectives on Power Control of AC Microgrid Considering Operation Cost and Efficiency. *IEEE Trans. Power Syst.* 36 (5), 4844–4847. doi:10.1109/tpwrs.2021.3080141

Yuan, W., Wang, Y., Liu, D., Deng, F., and Chen, Z. (2021). Efficiency-prioritized Droop Control Strategy of AC Microgrid. *IEEE J. Emerg. Sel. Top. Power Electron.* 9 (3), 2936–2950. doi:10.1109/jestpe.2020.2967756

Zhang, R., Sun, H., and Dong, X. (2019). The Comparison of Thermal Characteristics of AC Cable and DC cableJournal of Physics: Conference Series. *J. Phys. Conf. Ser.* 1187 (2), 022051. doi:10.1088/1742-6596/1187/2/022051